Research Square

Preprints are preliminary reports that have not undergone peer review.
They should not be considered conclusive, used to inform clinical practice,
or referenced by the media as validated information.

# Unraveling the mRNA-miRNA regulatory network of high photosynthetic efficiency to improve yield potential in Camellia oleifera

**Yanxiu Zhang**
Central South University of Forestry and Technology
**Xiaoling Ma**
fanxiaoling@163.com

Central South University of Forestry and Technology
**Xiangxiang Xu**
Central South University of Forestry and Technology
**Xinrui Liu**
Central South University of Forestry and Technology
**Deyi Yuan**
Central South University of Forestry and Technology

**Research Article**

**Keywords:** C. oleifera, high photosynthetic efficiency, mRNAs and miRNAs, ABA signaling, stomatal movement

**Posted Date:** November 19th, 2026

**DOI:** https://doi.org/10.21203/rs.3.rs-11429442/v1

**License:** This work is licensed under a Creative Commons Attribution 4.0 International License.
Read Full License

**Additional Declarations:** No competing interests reported.

# Abstract

*Camellia oleifera* Abel. (*C. oleifera*) is a premier woody oilseed tree species extensively cultivated in southern China. However, the widespread prevalence of low-yielding plantations severely restricts *C. oleifera* production. Improving photosynthetic efficiency represents a pivotal strategy for boosting production in *C. oleifera*. In this study, we selected a key hybrid population developed in our team, and performed leaf physiological and morphological measurements, mRNA-seq and miRNA-seq analyses on leaves from the parental cross YZ-2 × HY3 and five $F_1$ hybrid progenies. The results demonstrated that YH-5 and YH-10 exhibited high photosynthetic efficiency and high-parent heterosis., YH-1 fell below the low parents and YH-2, YH-4, YZ-2, and HY3 displayed intermediate photosynthetic efficiency. High photosynthetic efficiency of YH-5 and YH-10 relies on elevated light-harvesting efficiency, enhanced carbon fixation capacity, activated phytohormone signaling, enhanced stomatal movement and strengthened photoprotective mechanisms. Weighted gene co-expression network analysis identified four hub transcription factors-*BHLH63*, *HSFB1*, *NAC078* and *ARR2*-as putative regulators of net photosynthetic rate and pigment traits. Integrated miRNA and mRNA analysis revealed that miR393-x and novel-m0437-5p target *AFB2* and *BCA1* respectively, miR5282 target *CYP73A4*, highlighting that stomatal movement and photoprotection mechanisms play key roles in achieving high photosynthetic efficiency. Collectively, this study advances our understanding of the molecular mechanisms underlying high photosynthetic efficiency traits in *C. oleifera*, and provides a theoretical foundation for molecular breeding strategies targeting yield improvement.


# Introduction

*Camellia oleifera* Abel. (*C. oleifera*) is an important woody oil tree species endemic to southern China, highly valued for its premium edible *Camellia* oil, which is rich in unsaturated fatty acids [1]. *Camellia* oil has been reported to lower cholesterol, ameliorate cardiovascular and cerebrovascular diseases, enhance immunity, and scavenge free radicals [2, 3]. In recent years, *C. oleifera* has been widely cultivated in Hunan, Jiangxi, Guangxi, and other regions, and the *C. oleifera* industry has become a key sector for safeguarding national food and oil security, improving forestry-related economic returns, and promoting rural revitalization [4]. However, low-yield stands account for over 60% of the total planting area, which severely constrains *C. oleifera* yield.

The source-flow-sink system represents the core physiological framework underlying crop yield formation. It delineates the translocation and allocation of photosynthates to sink organs, and directly determines the conversion efficiency of crop photosynthetic potential into final agronomic yield [5, 6]. Building on this framework, research on photosynthetic physiological mechanisms and breeding strategies targeting crop yield improvement is collectively referred to as “high photosynthetic efficiency breeding” [7]. Substantial progress in high photosynthetic efficiency breeding has been achieved in major crops including rice (*Oryza sativa* L.), wheat (*Triticum aestivum* L.), potato (*Solanum tuberosum* L.), and soybean (*Glycine max* (L.) Merr.) [8–11]. Evaluation systems for photosynthetic traits and screening

protocols for elite germplasm have been established, and core photosynthetic traits have been defined, including chlorophyll content, net photosynthetic rate, stomatal conductance, transpiration rate, and leaf area [12–14]. With the continued advancement of high-throughput sequencing technologies, mRNA and miRNA sequencing have been increasingly applied in studies of high photosynthetic efficiency, enabling systematic dissection of the regulatory networks underlying photosynthesis at the molecular level. In poplar, the miR396a-GRF15 module was identified as a key regulatory node controlling photosynthetic efficiency [15]. In rice, several key genes associated with high photosynthetic efficiency, as well as the OsNF-YB7-miR5810-OsMRLP6 regulatory module, have been identified [16]. At present, research on high photosynthetic efficiency in *C. oleifera* has focused mainly on the optimization of cultivation practices [17], whereas the molecular mechanisms underlying the formation of high photosynthetic efficiency traits remain few research.

*C. oleifera* exhibits inherent limitations in photosynthetic performance, including a low $CO_2$ saturation point, a high $CO_2$ compensation point, pronounced photoinhibition, and overall low photosynthetic efficiency, which are important factors constraining its yield [18]. Germplasm innovation enables the improvement of key genetic traits and can enhance photosynthetic efficiency and yield potential [19]. Among breeding strategies, hybridization, particularly interspecific hybridization, has become an important approach for germplasm improvement in *C. oleifera* [20]. Prof. Deyi Yuan's group has long conducted systematic research on hybrid breeding and germplasm innovation in *C. oleifera*. From crosses between the *C. yuhsienensis* 'YZ-2' and 'DY-2', 43 elite lines with early flowering and enlarged floral organs were selected [21]. YH15, characterized by large fruits, thin pericarps, and a high fresh-seed yield, was selected from $F_1$ progeny derived from an interspecific cross between *C. yuhsienensis* and *C. oleifera* [22]. More recently, interspecific hybridization between 'YZ-2' and Hainan *C. oleifera* (HY 3) generated the YH germplasm series, which exhibited pronounced heterosis in floral and fruit traits. Notably, YH-10 showed transgressive superiority in disease resistance and fruit size [4]. These YH hybrid germplasms provide valuable materials for dissecting the physiological and molecular basis of superior hybrid performance, particularly the mechanisms regulating photosynthetic efficiency, a key determinant of yield potential.

In this study, leaves from superior offspring and parental individuals sharing the same genetic background were used as experimental materials to screen *C. oleifera* germplasm with high photosynthetic efficiency, identify the major candidate genes and miRNAs, and preliminarily elucidate the potential molecular mechanisms by which the miRNA-mRNA regulatory network contributes to the establishment of high photosynthetic efficiency.

## Materials and methods

# Plant material and growth conditions

The *C. oleifera* cultivar YZ-2, HY3 and 5 superior strains of $F_1$ hybrid (named YH-1, YH-2, YH-4, YH-5, YH-10) were used in this study, which grew well without disease and with similar growth potential, were planted in the Central South Forestry University of Science and Technology located in Changsha, China (28°10’ N, 113°23’ E). The same fertilizer and water management were conducted for plants. On June 7, 2023, leaves were sampled from 8-year-old parental plants and five 4-year-old hybrid progenies, performing to determine photosynthesis-related traits and the construction of high-throughput sequencing libraries.

## Measurement of the traits associated with photosynthesis

The photosynthetic parameters, including net photosynthetic rate (Pn), stomatal conductance (Gs), transpiration rate (Tr), maximum net photosynthetic rate (Pnmax), light compensation point (LCP), intercellular $CO_2$ concentration (Ci), water use efficiency (WUE), apparent quantum efficiency (AQE), and dark respiration rate (Rd), were measured and calculated using a Li-6400xt portable photosynthesis system (LI-COR Biosciences, Lincoln, NE, USA). The parameter settings were 1000 μmol photons $m^{-2}$ $s^{-1}$, 400 μmol $CO_2$ $mol^{-1}$ and flow rate of 500 μmol $s^{-1}$ [23]. Meanwhile the gradient of photosynthetically active radiation was set according to the protocol described by Wu et al [24]. The maximum quantum yield of photosystem Ⅱ (Fv/Fm), effective quantum yield of PSⅡ (Y(Ⅱ)), photochemical quenching coefficients (qL, qP), and non-photochemical quenching coefficients (qN, NPQ) were measured using a PAM-2500 portable chlorophyll fluorometer [25]. Chlorophyll content, including Chla, Chlb and carotenoid, were measured following Acetone Ethanol Mixture Method using a spectrophotometer, and the Chla/b ratio was calculated [26]. Prepare the leaves extract solution and measure its absorbance at wavelengths of 645 nm, 663 nm and 470 nm. The determination of leaf morphological characteristics was performed following established protocols, as described by Wang [27]. Genetic variation analysis was conducted on all leaf traits of five superior plants among the hybrid progenies, with the coefficient of variation and heterosis index calculated. The calculation formula was referenced from Wang [27].

## RNA preparation, transcriptome sequencing and gene functional annotation

Intact mature leaves were selected for molecular sequencing analyses, the total twenty-one samples were sent to Guangzhou GenoDx Biotechnology Co., Ltd. (Huangpu District, Guangzhou, China), where the libraries were produced and sequenced. The cDNA fragments of ~ 200 bp in length were selected using AMPure XP beads, followed by PCR amplification and purification to generate the library. The low-quality reads and adaptor sequences of the raw reads were removed using Fastp software, and clean reads were mapped to a reference genome using HISAT2 [28, 29]. The mapped reads were assembled by StringTie (v1.3.3b) using a reference-based approach [30]. The expression levels of the mapped and novel genes were calculated via the fragments per kilobase per million fragments mapped (FPKM) method.

A total of 21 samples were assigned to 10 comparison groups for comparative analysis (YH-1 vs YH-5, YH-1 vs YH-10, YH-2 vs YH-5, YH-2 vs YH-10, YH-4 vs YH-5, YH-4 vs YH-10, YZ-2 vs YH-5, YZ-2 vs YH-10, HY3 vs YH-5, HY3 vs YH-10). Differentially expressed genes (DEGs) were identified using DESeq2 software with the following thresholds: |log2 fold change|>2 and a false discovery rate (FDR) < 0.05 [31]. Gene function was annotated based on Gene Ontology (GO), and the Kyoto Encyclopedia of Genes and Genomes (KEGG). GO term and KEGG pathway with a corrected $P < 0.05$ were defined as significantly enriched. The OmicShare platform (http://www.omicshare.com/tools) was used to predict transcription factors (TFs) from the sequencing data.

## Weighted gene co-expression network analysis and qRT-PCR

To identify the modules of highly correlated genes that were closely associated with sample traits (Pn and chlorophyll content), weighted gene co-expression network analysis was performed on genes with (FPKM ≥ 5). TFs and the values of all sample traits were predicted using the OmicShare platform with the default settings (power value = 7). The associations between trait and modules were estimated using spearman correlation coefficient between phenotype and module eigengenes. To screen the hub genes in important modules and create the interaction network, we selected genes with module membership ≥ 0.8, gene significance > 0.5, and those ranked in the top 5% by Kin value, then visualized them using Cytoscape [32].

DEGs with vital functions and high expression abundance were selected for qRT-PCR analysis. Gene-specific primers for qRT-PCR were designed using Primer 3plus software and synthesized by Tsingke Biotechnology Co., Ltd (Beijing). The qRT-PCR analysis was performed using the LightCycler 480 system (Roche, Basel, Switzerland) with the SYBR Green I Master Kit (Roche, Basel, Switzerland). CoEF1α (elongation factor 1α) was used as the internal reference control [33]. The specific primers for qRT-PCR are listed in Table S1. The relative expression levels of selected genes were calculated using the $2^{[-\Delta\Delta C(T)]}$ method [34].

## miRNA sequencing, target gene prediction and analysis

Total RNA was extracted from the samples using the TRIzol method. For sRNA library construction, the sRNA fractions with the length of 18–30 nt were purified from polyacrylamide gel. cDNA was synthesized by RT-PCR following the Illumina protocol. The bands of approximately 140 bp were recovered by gel extraction, purified, and dissolved in EB solution to complete library construction. Low-quality data were filtered out, and miRNAs were identified using Bowtie (version 1.1.2) and miRDeep2 software with miRBase as the reference. The method for identifying differentially expressed miRNAs was the same as that for identifying mRNAs.

The patmatch_v1.2 software was used for complementary pairing between miRNAs and target genes, and the predicted results were further filtered through a program to obtain the final outcomes. To

uncover the miRNA-gene regulatory network on the basis of biological process and molecular function, the Gene Ontology (GO) and the Kyoto Encyclopedia of Genes and Genomes (KEGG) analysis of the candidate target transcripts was performed.

# miRNA-mRNA interaction network analysis

By integrating the differential expression results of miRNAs and their target genes as well as the analysis results of their targeting relationships, the Pearson correlation coefficients between miRNAs and target genes were calculated. miRNA-target gene pairs with negatively correlated expression levels were screened out based on the criteria of correlation coefficient < -0.5 and p-value < 0.05. miRNA-mRNA interaction network was further constructed and visualized using Cytoscape software.

# Statistical analysis

All results are presented as mean ± standard error (SE), with three biological replicates per experiment. The statistical analysis of the data was performed using one-way ANOVA with the GraphPad Prism 10 (GraphPad Software, San Diego, CA, USA). Different lowercase letters indicate significant differences at the $P < 0.05$ level.

## Results

# Analysis of leaf phenotypic traits and heterosis

To clarify the variation in high photosynthetic efficiency traits among *C. oleifera* parents and their hybrid progenies (YZ-2, HY3, YH-1, YH-2, YH-4, YH-5, YH-10), we systematically measured leaf photosynthetic parameters (Gas exchange parameters, Light response curve parameters, Chlorophyll fluorescence parameters), pigment contents, and leaf morphological traits (Table S2, Fig. 1). The results revealed abundant genetic variation in leaf traits among individual hybrid progenies, with CV ranging from 2.18% to 55.12%, and HI exhibits substantial variation across distinct traits (58.71%-195.38%; Table S2). We evaluated all plants using indicators which are representative traits of high photosynthetic efficiency, with CV > 10% and indicating pronounced heterosis (Pn, Gs, Tr, Pnmax, LCP, Chla, Chlb, Cha/b and carteniod). The results showed YH-5 and YH-10 showed significantly better overall performance than the other individuals, whereas YH-1 exhibited the poorest performance. What's more, both YH-5 and YH-10 outperformed the parental lines in several high light efficiency traits (Fig. 1). The Pn values of YH-5 and YH-10 were 171.22% and 170.10% higher than that of YH-1, and 32.99% and 32.44% higher than those of the superior parent, respectively. Similarly, Gs in YH-5 and YH-10 was 136.99% higher than that in YH-1 and 71.61% higher than that in the superior parent. For Pnmax, YH-5 and YH-10 exceeded YH-1 by 74.17% and 109.22%, respectively, and surpassed the superior parent by 0.35% and 20.54%, respectively (Table S2). Chla and Chlb contents in YH-5 and YH-10 exhibited pronounced better-parent heterosis. The Chla/b ratio peaked in YH-5, while that of YH-10 was slightly lower but remained at a relatively high level. Carotenoid contents in YH-5 and YH-10 were also significantly higher than those in the other progeny

lines. In conclusion, YH-5 and YH-10 generally showed superior performance in traits, whereas YH-1 served as an extreme low-value line and the remaining progenies presented intermediate phenotypes.

# Characterization of the transcriptomes and identification of DEGs

To elucidate the molecular mechanisms underlying the formation of high photosynthetic efficiency traits in *C. oleifera* leaves, we performed transcriptome sequencing on 21 submitted samples. From the leaf samples submitted for transcriptome sequencing, we generated a total of 874,448,314 raw reads. Following quality control (QC) filtering, 871,049,970 high-quality clean reads were retained, with Q30 scores exceeding 93.13%. Mapping the clean reads sequences to the *C. oleifera* reference genome, the proportion of mapped reads per library ranged from 79.93% to 85.27%, and a total of 60,181 expressed unigenes (Table S3). The assembly quality of the transcriptome was rated as satisfactory. There were 29,146 unigenes with FPKM values of ≥ 1.5. PCA of the 21 samples suggested that the biological reproducibility among samples was excellent (Figure S1). These results supported our subsequent transcriptome analysis. Among the 10 comparison groups, 12,068 DEGs were identified in total. The YZ-2 vs YH-10 comparison yielded the largest number of DEGs (6212; 2876 up-regulated and 3336 down-regulated), whereas YH-2 vs YH-5 exhibited fewest (1834; 922 up-regulated and 912 down-regulated) in Fig. 2A. The 10 comparisons were classified into three groups: Group A, high vs low photosynthetic-efficiency individuals; Group B, high vs intermediate photosynthetic-efficiency individuals; Group C, high photosynthetic efficiency individuals vs. parental lines. Venn diagram analysis identified 953 common DEGs in Group A, 213 in Group B, and 462 in Group C (Fig. 2B).

GO and KEGG enrichment analyses were performed to explore the functional characteristics of all DEGs. These DEGs were assigned to three core GO categories. Within the biological process category, the most enriched GO terms were dominated by cellular process and metabolic process, followed by biological regulation, response to stimulus, and regulation of biological process. In the molecular function category, the top three terms were binding, catalytic activity and transporter activity. For the cellular component category, the terms included cellular anatomical entity and protein-containing complex (Figure S2A). KEGG enrichment analysis demonstrated significant enrichment of DEGs in flavonoid biosynthesis, phenylpropanoid biosynthesis, starch and sucrose metabolism, carotenoid biosynthesis and glutathione metabolism (Figure S2B). Moreover, a subset of DEGs were also enriched in pathways including photosynthesis-antenna proteins, carbon fixation in photosynthetic organisms, nitrogen metabolism, plant hormone signal transduction, and MAPK signaling pathway.

# Identification of key DEGs involved in high photosynthetic efficiency

# Key DEGs associated with photosynthetic core pathways

KEGG enrichment analysis identified three pathways directly related to photosynthetic performance, namely Photosynthesis-antenna proteins, Carbon fixation in photosynthetic organism, and Carotenoid biosynthesis. In the Photosynthesis-antenna protein pathway, six DEGs encoding light-harvesting chlorophyll-binding proteins for LHCII assembly were identified, including *CAB13-1*, *CAB13-2*, *CAB21*, *CAB40*, *LHCB3*, *CAP10A*. These genes had the lowest expression in YH-1 and reached maximum levels in YH-10, except the expression level of *CAB21* was lower than the high parental line. Notably, the expression of *CAB13* in YH-10 was 917.39% higher than YH-1, and 280.43% higher than that in the high parent (Fig. 3A). These results indicate that YH-10 achieves an enhanced light-harvesting capacity through upregulation of *LHCB* genes. A large number of DEGs were also enriched in the Carbon fixation in photosynthetic organism pathway. Particularly, the expression levels of *RBCS-1A* (encoding the Rubisco small subunit) were upregulated in YH-5 and YH-10 compared with the other progeny. *SBPase* was a key rate-limiting enzyme in the Calvin cycle, it showed the highest expression in YH-5 (258.81% higher than the lowest level in YH-1) and maintained intermediate levels in the other plants. *GAPC* was also up-regulated in YH-5 and YH-10 leaves compared with YH-1 (Fig. 3A). The Carotenoid biosynthesis pathway was enriched with five DEGs, including *CCD4-1*, *CCD4-2*, *CYP707A1*, *CYP707A2*, and *AOG*. They were significantly up-regulated in YH-5 and YH-10 compared with YH-1. Notably, *CCD4-1* and *CCD4-2* exhibited a clear transgressive expression pattern in YH-5 and YH-10, with transcript abundance surpassing that of both parents and all other progeny examined. (Fig. 3A). Functional annotation indicated that these genes are associated with carotenoid cleavage and ABA metabolism.

# Key DEGs associated with hormone-related

Phytohormones serve as central regulators of leaf development, stomatal dynamics, chloroplast function, and stress acclimation, playing crucial roles in determining photosynthetic efficiency [35]. KEGG enrichment analysis revealed that a substantial number of DEGs were significantly enriched in hormone-related pathways, encompassing the auxin, cytokinin, jasmonate, abscisic acid, gibberellin, and brassinosteroid. Based on their expression profiles, these DEGs were primarily categorized into two distinct regulatory modules (Fig. 3B). Within the up-regulated module, genes including *PYL4*, two *MYC2*, *BSK2*, *RBOHC*, *BEH2* and *ERL2* exhibited significantly higher transcript abundance in YH-5 and YH-10 compared with YH-1. Notably, most up-regulated DEGs exhibited pronounced transgressive expression in YH-10. Representative genes include *MYC2* and *BEH2*, key TFs in JA and BR signaling, as well as the ABA receptor gene *PYL4*. *RBOHC*, an essential gene for reactive oxygen species (ROS) production that mediates stomatal movement, exhibited higher transcript levels in YH-5 and YH-10 than in the other progeny lines. Conversely, *IAA13*, *IAA26*, *PP2C06*, two *PP2C24*, *MPK3*, and *ARR2* exhibited transcriptional suppression in YH-5 and YH-10. *IAA13* and *IAA26* encode Aux/IAA repressor proteins. Specifically, the expression of *IAA13* in YH-5 and YH-10 was reduced by 80.08% and 69.18%, respectively, compared with YH-1. Three PP2C family genes were negative regulators of ABA signaling. They exhibited extremely low expression in YH-5 and YH-10 but showed markedly high expression in YH-1. Interestingly, *ARR2*, a type-B response regulator acting as a transcription factor in cytokinin signaling, also displayed a low expression

pattern in the YH-5 and YH-10. These results demonstrate that phytohormones play a role in regulating the high photosynthetic efficiency in leaves.

# Other important DEGs associated with high photosynthetic efficiency

Photoprotective mechanisms and carbon-nitrogen metabolic coordination jointly contribute to the establishment of the high photosynthetic efficiency trait [36, 37]. Within the Glutathione metabolism pathway, members of the glutathione S-transferase (GSTU) family exhibited divergent expression profiles; *GSTU7* and *GSTU22* were significantly up-regulated in the high photosynthetic efficiency leaves, whereas *GSTU17* was down-regulated. Distinct genes within the GSTU family exhibit pronounced functional divergence. Furthermore, *CICDH* (encoding cytosolic isocitrate dehydrogenase) and the chloroplast-localized *HSP26-A* displayed markedly higher transcript abundance in the YH-5 and YH-10 (Fig. 3C). Genes encoding rate-limiting enzymes in the Phenylpropanoid biosynthesis and Flavonoid biosynthesis pathways, including *CHS*, *CAD6*, *4CL3*, *CYP73A4*, *SHT*, and *LAR*, were differentially expressed between high- and low photosynthetic efficiency leaves. In the Starch and sucrose metabolism pathway, genes governing starch biosynthesis (*AGPS1* and *WAXY*), β-amylase 1 (*BAM1*) and starch phosphorylase (*PHO1*), were significantly down-regulated in YH-5 and YH-10. Conversely, *BAM3* (responsible for chloroplast starch degradation) and *INV*DC4* (essential for sucrose hydrolysis) exhibited pronounced up-regulation. Concurrently, within the Nitrogen metabolism pathway, three *BCA1* (beta-carbonic anhydrase 1) genes were sharply up-regulated in YH-5 and YH-10 (Fig. 3C).

# Weighted gene co-expression network analysis and qRT-PCR

The expressed genes were clustered into 15 distinct co-expression modules, with module sizes ranging from 64 (indianred4) to 9,540 (yellow4) genes. Notably, only 5 genes (accounting for a mere 0.025% of the total) remained unassigned (grey module), underscoring the high reliability of the network construction (Fig. 4A-B). Among them, darkseagreen3, green, navajowhite1, blue2 and darkviolet were strongly correlated with phenotypic traits ($r > 0.60$) (Fig. 4C). These modules are significantly enriched for genes associated with photosynthetic processes (Figure S3). TFs *bHLH63* and *HSFB1*, together with genes *HSP26-A* and *GSTU7* were identified as hub positive regulators. TFs *NAC078* and *ARR2*, along with genes *PHO1*, *IAA13*, *PP2C06* and *BAM1*, were identified as hub negative regulators (Fig. 5).

To validate the reliability of the RNA-seq data, nine key DEGs associated with high photosynthetic efficiency were subjected to qRT-PCR analysis. The expression patterns of these genes were consistent with the transcriptome results (Fig. 6).

# miRNA sequencing, differentially expressed miRNAs analysis and Target prediction

High-throughput Illumina sequencing of the miRNA libraries generated raw reads. Following the filtration of low-quality sequences, a total of 236,461,925 clean reads were retained. To identify conserved miRNAs, these size-selected reads were mapped onto the *C. oleifera* reference genome. The mapped sequences were subsequently aligned against known precursor and mature miRNA sequences in the miRBase repository (Release 20.0). This resulted in the identification of 482 known miRNAs. Furthermore, de novo prediction utilizing the miRDeep2 software yielded 1,254 novel miRNA candidates. Differential expression analysis identified a total of 850 differentially expressed miRNAs (DEMs), comprising 118 known and 732 novel miRNAs (Table S5).

Target gene prediction and KEGG enrichment analysis of the DEMs revealed that target genes were predominantly mapped to pathways such as “Basal transcription factors”, “Plant-pathogen interaction”, “Starch and sucrose metabolism” and “Plant hormone signal transduction” (Figure S4). The prediction results indicate that, miR1511-y was predicted to target 61 distinct genes, including *ARR-B* and *WRKY* TFs, involving multiple biological processes. miR8175-z primarily modulates phytohormone signaling and starch and sucrose metabolism, directly targeting key components like *PP2CA* and *INV*DC4*, hinting at its vital role in mediating carbon partitioning. Furthermore, miR5054-z targets the critical receptor *PYL4* and *ERF* (TFs), and miR156-x targets a massive array of *SBP* TFs. These miRNAs targeted photosynthesis-related DEGs, implying their potential roles in the development of high photosynthetic efficiency traits (Fig. 7A).

# Construction of miRNA-mRNA interaction network

Based on expression profiling and strict target prediction algorithms, we constructed a global miRNA-mRNA interaction network for all DEMs and target genes (Fig. 7B). We screened 23 miRNA-mRNA pairs, involving 20 DEMs and 22 DEGs. Targets contained five photosynthetic performance-related genes, including *BCA1*, *PIP2-5*, *CYP73A4*, *ALDH2B7* and AFB2. Specifically, the carbon assimilation-related *BCA1* was a target of novel-m0437-5p, the aquaporin *PIP2-5* was targeted by miR8155-z, the cinnamate-4-hydroxylase *CYP73A4* was a target of miR5282-z, the aldehyde dehydrogenase *ALDH2B7* was targeted by miR5059, the auxin receptor *AFB2* was targeted by miR393-x.

## Discussion

Generating segregating populations with uniform genetic backgrounds via hybridization is a pivotal strategy for genetic improvement and precision molecular breeding [38]. Previous studies have used different *C. oleifera* cultivars as materials to screen key genes underlying inter-cultivar differences in leaf photosynthetic efficiency [39]. However, the extensive genetic heterogeneity among cultivars hinders the accurate identification of key regulators of photosynthetic traits. In this study, we used the hexaploid and decaploid parents of *C. oleifera*, together with progeny plants with high, medium and low photosynthetic efficiency from the hybrid population as experimental materials. This effectively minimizes the confounding effects derived from inter-cultivar genetic differences. Meanwhile, we referred to the universal evaluation indicators for high photosynthetic efficiency breeding across multiple species,

combined with the coefficient of variation and heterosis index of various leaf photosynthesis-related parameters in the experimental population (Table S2). We selected leaf physiological indicators with strong representativeness and abundant variation for research, ensuring the scientific rigor of subsequent studies.

Enhancements in photosynthetic efficiency stem from the optimized coordination of photosystem architecture, light harvesting, electron transport, Rubisco carboxylation, photoprotection, and photosynthate export [40–42]. This study found that high photosynthetic efficiency leaves (YH-5 and YH-10) were characterized by higher light-harvesting efficiency (LHCB), enhanced carbon fixation capacity (RBCS, SBPase etc.), activated phytohormone signaling regulation (IAA, ABA etc.), and reinforced photoprotective mechanisms (GSTU, HSP etc.). Notably, RBCS and SBPase act at two key nodes of the Calvin cycle—carboxylation capacity and substrate regeneration, respectively. They play critical regulatory roles in photosynthetic capacity and carbon use efficiency [43, 44, 36]. In this study, the coordinated upregulation of *RBCS-1A* and *SBPase* in high photosynthetic efficiency leaves likely enhanced Calvin–Benson cycle flux, thereby improving carbon-use efficiency. As a core regulatory phytohormone of stomatal movement, ABA plays a critical role in determining the rate of photosynthetic carbon assimilation [40]. In higher plants, ABA is predominantly synthesized through the carotenoid cleavage pathway, which serves as a key metabolic link between carotenoid metabolism and stomatal regulation [45]. Upregulation of the carotenoid cleavage dioxygenase CCD4 has been reported to enhance photosynthetic and photoprotective efficiency, as well as promoting ABA biosynthesis in plants [46, 47]. Consistently, our study identified differential expression of CCD4 and a suite of genes involved in ABA metabolism and stomatal regulation (*CYP707As*, *PYL4*, *PP2Cs*, *RBOHC*, *BAM1* and *BCA1*) in high photosynthetic efficiency leaves. These coordinated transcriptional changes suggest that enhanced carotenoid metabolism and ABA signaling may facilitate dynamic stomatal regulation, thereby promoting $CO_2$ assimilation while maintaining effective photoprotection.

WGCNA revealed *bHLH63* as a positive regulatory hub TF, a finding consistent with previous reports in rapeseed that bHLH63 regulates photosynthesis-related genes and may be involved in maintaining photosynthetic efficiency [48]. *NAC078* has been closely associated with leaf senescence [49]. In this study, *NAC078* emerged as a core negatively regulated TF, implying that its reduced activity may contribute to delayed leaf senescence and thereby prolong photosynthetic longevity. Notably, previous studies have shown that heat shock factors (HSFs) can bind the *HSP21.9* promoter, modulate PSI and PSII core subunits and light-harvesting complex proteins, and increase glutathione levels, thereby alleviating heat and high light induced photoinhibition [50, 51]. In our study, the hub TF *HSFB1* was closely co-expressed with *HSP26-A* and *GSTU7*, suggesting that an HSFB1 centered module may coordinate protein protection and redox homeostasis to maintain photosynthetic apparatus stability.

MicroRNAs (miRNAs) regulate gene transcription and participate in diverse biological processes in *C. oleifera*, including oil biosynthesis, stress responses, growth, and development [52, 39]. However, the miRNA-mediated mechanisms underlying high photosynthetic efficiency in *C. oleifera* remain poorly

understood. Our integrated analysis identified several miRNA-mRNA modules associated with high photosynthetic efficiency in *C. oleifera* leaves. miR393 is a key regulator of auxin signaling that modulates plant growth, development, and stress responses by targeting genes encoding the transport inhibitor TIR1/AFB auxin receptors [53]. TIR1/AFB acts as a negative regulator of stomatal development, and AFB2 overexpression in tomato causes leaf curling and decreased stomatal density [54.55]. Consistently, our research found miR393-x targets *AFB2*, and *AFB2* was downregulated in leaves with high photosynthetic efficiency. We hypothesized that the module may promote stomatal development, thereby contributing to photosynthetic efficiency. *BCA1* encodes the chloroplast β-carbonic anhydrase 1, which was an upstream regulator of $CO_2$-controlled stomatal movements in guard cells [56]. We identified a novel miRNA, novel-m0437-5p, that targets *BCA1*. This regulatory module may influence photosynthetic efficiency by modulating stomatal movement, providing new candidate targets for the genetic improvement of *C. oleifera*. miR5282 targets glutathione S-transferase (GST) genes involved in reactive oxygen species (ROS) homeostasis [57]. Here, miR5282-z was predicted to target *CYP73A4*, inferring that this module may be associated with photoprotection. miR5059 has been commonly used as a stable reference for miRNA qRT-PCR analysis [58, 59]. However, in the present study, miR5059-z was significantly upregulated in high photosynthetic efficiency leaves. These results indicate that stomatal movement and photoprotective mechanisms play important roles in high photosynthetic efficiency.

# Conclusion

We identified plants that high photosynthetic efficiency over parents (YH-5, YH-10), fell below the low parents (YH-1), and were intermediate in photosynthetic efficiency (YH-2, YH-4, YZ-2, HY3), by integrating leaf physiological and morphological traits from a hybrid population. Transcriptome analyses revealed high photosynthetic efficiency were affected by coordinated regulation of the differential expression genes with light-harvesting (*CAB13*, *LHCB3*), photosynthetic carbon fixation (*RBCS-1A*, *SBPase*), stomatal movement (*PP2C06*, *BCA1)*, phytohormone signaling (*CCD4*, *MPK3*) and photoprotection (*HSP26-A*, *GSTU7*). Thereinto, enhanced carotenoid metabolism activated ABA signaling, which jointly modulated stomatal movement and increased photosynthetic efficiency. *BHLH63*, *HSFB1*, *NAC078* and *ARR2* were hub TFs that regulates chlorophyll content and Pn. Integrated miRNA-mRNA analysis identified three modules: miR393-x - *AFB2*, novel-m0437-5p - *BCA1* and miR5282 - *CYP73A4*, highlighting the importance of stomatal and photoprotection (Fig. 8). These findings advance understanding of the molecular network underlying high photosynthetic efficiency in *C. oleifera* and provide a basis for molecular breeding to improve its production.

# Declarations

### Ethics approval and consent to participate

Not applicable.

### Consent for publication

Not applicable.

**Availability of data and material**

Supporting data of Additional files 1-2 are included as additional files in the manuscript.

**Competing interests**

The authors declare that there are no competing interests.

**Funding**

This work was supported by the Yuelushan Laboratory Breeding Program (YLS-2025-ZY02050), the National Natural Science Foundation of China (32602634), Top Ten Technical Research Projects in Hunan Province (2024NK1020), the Key Program of Education Department of Hunan Province (24A0215), and Scientific Research Foundation for Advanced Talents of Central South University of Forestry and Technology (2019YJ003).

**Author' contributions**

Xiaoling Ma and Deyi Yuan designed the research. Deyi Yuan provided the *C. oleifera* samples. Yanxiu Zhang and Xiaoling Ma mainly performed the research. Xiangxiang Xu and Xinrui Liu finished some parts of the experiments. Xiaoling Ma and Yanxiu Zhang analyzed the data. Yanxiu Zhang wrote the manuscript. Xiaoling Ma and Deyi Yuan revised and approved the manuscript. All authors read and agreed to the published version of the manuscript.

**Acknowledgments**

We thank Weiqi Wang (Central South University of Forestry and Technology) for experimental guidance and data analysis of this manuscript. We are also grateful to the reviewers for their constructive comments on the revision of the manuscript.

# References

1. Lin P, Wang KL, Wang YP, et al. The genome of oil-Camellia and population genomics analysis provide insights into seed oil domestication. Genome Biol. 2022;23(1):14.
2. Guo N, Tong TT, Ren N, et al. Saponins from seeds of Genus Camellia: phytochemistry and bioactivity. Phytochemistry. 2018;149:42–55.
3. Zhu XY, Lin HM, Chen X, et al. Mechanochemical-assisted extraction and antioxidant activities of kaempferol glycosides from *Camellia oleifera* Abel. meal. J Agric Food Chem. 2011;59(8):3986–93.
4. Ma XL, Yuan DY, Wang WQ, et al. Comparison of Flower and Fruit Traits of Superior $F_1$ Hybrids among Camellia Species. J Cent South Univ Forestry Technol. 2026;46(5):1–11.

5. Ainsworth EA, Long SP. What have we learned from 15 years of free-air CO2 enrichment (FACE)? A meta-analytic review of the responses of photosynthesis, canopy properties and plant production to rising CO2. New Phytol. 2005;165(2):351–71.
6. Chang TG, Wei ZW, Shi Z, et al. Bridging photosynthesis and crop yield formation with a mechanistic model of whole-plant carbon-nitrogen interaction. silico Plants. 2023;5:1–19.
7. Wang R, Chen YZ. Discussion on high light-efficiency breeding and cultivation techniques of *Camellia oleifera*. Forestry Sci Technol. 2011;25(3):1–4.
8. Shen QP, Xie YJ, Qiu XZ, et al. The era of cultivating smart rice with high light efficiency and heat tolerance has come of age. Front Plant Sci. 2022;13:1021203.
9. Ru ZG, Feng SW, Li G. High-yield potential and effective ways of wheat in the Yellow and Huai River valley facultative winter wheat region. Scientia Agricultura Sinica. 2015;48(17):3388–93.
10. Li CB, Guo HC. Evaluation of low-light tolerance and screening of indicators in potato varieties. Scientia Agricultura Sinica. 2017;50(18):3461–72.
11. Niu N, Li ZX, Jin SJ, et al. Photosynthetic characteristics and screening of high light-efficiency germplasm of soybean in the Huang-Huai-Hai region. Chin J Oil Crop Sci. 2018;40(4):524–32.
12. Wang MG, Xu LH, Zhang YM, et al. Analysis of photosynthetic characteristics and screening of high light-efficiency germplasm in soybean. Plant Sci. 2025;43(6):781–9.
13. Guo R, Wang SF, Cheng J, et al. Identification methods and screening of high light-efficiency materials in wheat. Seed. 2026;45(3):112–7.
14. Acevedo-Siaca LG, Coe R, Wang Y, et al. Variation in photosynthetic induction between rice accessions and its potential for improving productivity. New Phytol. 2020;227(4):1097–108.
15. Zhao YY, Xie JB, Wang S, et al. Synonymous mutation in *Growth Regulating Factor 15* of miR396a target sites enhances photosynthetic efficiency and heat tolerance in poplar. J Exp Bot. 2021;72(12):4502–19.
16. Gao WW, Li MK, Cheng HP, et al. The miR5810/OsMRLP6 regulatory module affects rice seedling photosynthesis. Crop J. 2023;11(6):1686–95.
17. Si YY, Lu YF, Bai YJ, et al. The Combination of High-Light Efficiency Pruning and Mulching Improves Fruit Quality and Uneven Maturation at Harvest in *Camellia oleifera*. Horticulturae. 2024;10(4):343.
18. Chen LS, Chen YZ, Peng SF. Research progress in photosynthetic characteristics and prospects of high light-efficiency breeding in Camellia oleifera. Hunan Forestry Sci Technol. 2010;37(3):33–9.
19. Sharwood RE, Quick WP, Sargent D, et al. Mining for allelic gold: finding genetic variation in photosynthetic traits in crops and wild relatives. J Exp Bot. 2022;73(10):ERAC081.
20. Gong H, Chang YH, Xu JM et al. 2023. Unilateral cross-incompatibility between *Camellia oleifera* and *C. yuhsienensis* provides new insights for hybridization in *Camellia spp*. Frontiers in plant science. 14, 1182745.
21. Li NX, Jiang Y, Yuan Y, et al. Analysis of Flowering Period and Floral Organ Traits Variation in Inter-Specific Hybrid Offspring of *Camellia Oleifera*. J For Environ. 2024;44(2):183–9.

22. Chen Y. Comparative Analysis of Major Traits in 18 Superior Individuals of $F_1$ Generation from Interspecific Hybridization of *Camellia oleifera*. Changsha: Central South University of Forestry and Technology; 2020.
23. He Z, Liu C, Wang X, Wang R, Tian Y, Chen Y. Leaf transcriptome and weighted gene co-expression network analysis uncovers genes associated with photosynthetic efficiency in *Camellia oleifera*. Biochem Genet. 2020;59:398–421.
24. Wu FY, Li Z, Liu FD, et al. Comparison of photosynthetic characteristics of main cultivated varieties of *Camellia oleifera*. Non-wood For Res. 2018;36(2):7–13.
25. Zhu YX, Yang W, Luo YJ, et al. Analysis of photosynthetic characteristics and chlorophyll fluorescence parameters of tea leaves under different forest canopies in ancient tea plantations of Jingmai Mountain. Jiangsu Agricultural Sci. 2023;51(22):138–44.
26. Du L. Research on the Optimization of Cultivation Technology for Green Bamboo Container Seedlings. Beijing: Chinese Academy of Forestry; 2019.
27. Wang WQ. Comparative analysis of main traits of 10 superior plants in the $F_1$ generation of a 'Youza 2' x 'Haiyou 3' cross. Changsha: Central South University of Forestry and Technology; 2024.
28. Chen SF, Zhou YQ, Chen YR, et al. fastp: an ultra-fast all-in-one FASTQ preprocessor. Bioinf (Oxford England). 2018;34(17):i884–90.
29. Kim D, Langmead B, Salzberg SL. HISAT: a fast spliced aligner with low memory requirements. Nat Methods. 2015;12(4):357–60.
30. Pertea M, Pertea GM, Antonescu CM, et al. StringTie enables improved reconstruction of a transcriptome from RNA-seq reads. Nat Biotechnol. 2015;33(3):290–5.
31. Love MI, Huber W, Anders S. Moderated estimation of fold change and dispersion for RNA-seq data with DESeq2. Genome Biol. 2014;15(12):550.
32. Shannon P, Markiel A, Ozier O, et al. Cytoscape: a software environment for integrated models of biomolecular interaction networks. Genome Res. 2003;13(11):2498–504.
33. Hu X, Yang M, Gong SF, et al. Ethylene-regulated immature fruit abscission is associated with higher expression of *CoACO* genes in *Camellia oleifera*. Royal Soc Open Sci. 2021;8(6):202340.
34. Livak KJ, Schmittgen TD. Analysis of relative gene expression data using real-time quantitative PCR and the 2-delta delta CT method. Methods. 2001;25:402–8.
35. Müller M, Munné-Bosch S. Hormonal impact on photosynthesis and photoprotection in plants. Plant Physiol. 2021;185(4):1500–22.
36. Zhang SQ, Li XH, Wang XY, et al. Optimizing source-sink relationships and photoprotective mechanisms in wheat to enhance photosynthetic efficiency and nitrogen management. Front Plant Sci. 2025;16:1660834.
37. Liu H, Gao XH, Fan WS, et al. Optimizing carbon and nitrogen metabolism in plants: from fundamental principles to practical applications. J Integr Plant Biol. 2025;67(6):1447–66.

38. Kumar A, Sandhu N, Venkateshwarlu C, et al. Development of introgression lines in high yielding, semi-dwarf genetic backgrounds to enable improvement of modern rice varieties for tolerance to multiple abiotic stresses free from undesirable linkage drag. Sci Rep. 2020;10(1):13073.
39. He ZL, Liu CX, Zhang Z, et al. Integration of mRNA and miRNA analysis reveals the differentially regulatory network in two different Camellia oleifera cultivars under drought stress. Front Plant Sci. 2022;13:1001357.
40. Croce R, Silva CE, Cho BY, et al. Perspectives on improving photosynthesis to increase crop yield. Plant Cell. 2024;36:3944–73.
41. Liu YH, Chen JM, He LM, et al. Global photosynthetic capacity of C3 biomes retrieved from solar-induced chlorophyll fluorescence and leaf chlorophyll content. Remote Sens Environ. 2023;287:113457.
42. Miri H. Changes in grain yield and associated physiological traits in Iranian wheat (Triticum aestivum L.) cultivars released during 1940–2000. J Sci Technol Agric Nat Resour. 2009;12(46):43.
43. Zhang SQ, Sun JW, Lu YH et al. 2024. Rubisco and sucrose synthesis and translocation are involved in the regulation of photosynthesis in wheat with different source-sink relationships. Physiol Plant. 176(2), e14196.
44. Ding F, Wang ML, Zhang SX, et al. Changes in SBPase activity influence photosynthetic capacity, growth, and tolerance to chilling stress in transgenic tomato plants. Sci Rep. 2016;6(1):32741.
45. Marusig D, Tombesi S. Abscisic acid mediates drought and salt stress responses in *Vitis vinifera*-A review. Int J Mol Sci. 2020;21(22):8648.
46. Tian Q, Han W, Zhou S, et al. Carotenoid cleavage dioxygenase gene CCD4 enhances tanshinone accumulation and drought resistance in Salvia miltiorrhiza. Int J Mol Sci. 2024;25(23):13223.
47. Ke QB, Kang L, Kim HS, et al. Down-regulation of *lycopene ε-cyclase* expression in transgenic sweetpotato plants increases the carotenoid content and tolerance to abiotic stress. Plant Sci. 2019;281:52–60.
48. Shahsavari M, Raspor M, Mohammadi V. Genome-wide transcriptional analysis of rapeseed (*Brassica napus L.*) responses to heat stress: an integrated RNA-Seq meta-analysis, gene co-expression, and gene regulatory network study. BMC Plant Biol. 2025;26:73.
49. Wang CC, Liao GH, Duan LY, et al. Identification of NAC transcription factors associated with leaf senescence in *Clerodendrum japonicum*. Int J Mol Sci. 2025;26(18):8846.
50. Andrási N, Pettkó-Szandtner A, Szabados L. Diversity of plant heat shock factors: regulation, interactions, and functions. J Exp Bot. 2020;72(5):1558–75.
51. Singh RK, Muthamilarasan M, Prasad M. SiHSFA2e regulated expression of SisHSP21.9 maintains chloroplast proteome integrity under high temperature stress. Cell Mol Life Sci. 2022;79:580.
52. Wu B, Ruan CJ, Shah AH, et al. Identification of miRNA-mRNA Regulatory Modules Involved in Lipid Metabolism and Seed Development in a Woody Oil Tree (*Camellia oleifera*). Cells. 2021;11(1):71.

53. Jiang JJ, Zhu HT, Li N, et al. The miR393-Target Module regulates plant development and responses to biotic and abiotic stresses. Int J Mol Sci. 2022;23(16):9477.
54. Zhang JY, He SB, Li L, et al. Auxin inhibits stomatal development through MONOPTEROS repression of a mobile peptide gene *STOMAGEN* in mesophyll. Proc Natl Acad Sci USA. 2014;111(29):E3015–23.
55. Xu J, Li J, Cui L, et al. New insights into the roles of cucumber TIR1 homologs and miR393 in regulating fruit/seed set development and leaf morphogenesis. BMC Plant Biol. 2017;17(1):130.
56. Hu HH, Boisson-Dernier A, Israelsson- Nordström M, et al. Carbonic anhydrases are upstream regulators of CO2-controlled stomatal movements in guard cells. Nat Cell Biol. 2011;13(6):734.
57. Devers EA, Branscheid A, May P, et al. MicroRNA- and MicroRNA*-Mediated Transcript Cleavage Involved in Arbuscular Mycorrhizal Symbiosis. Plant Physiol. 2011;156(4):1990–2010.
58. Li SX, Shao ZR, Fu XL, et al. Identification and characterization of *Prunus persica* miRNAs in response to UVB radiation in greenhouse through high-throughput sequencing. BMC Genomics. 2017;18:938.
59. Yang YT, Zhang X, Chen Y, et al. Selection of Reference Genes for Normalization of MicroRNA Expression by RT-qPCR in Sugarcane Buds under Cold Stress. Front Plant Sci. 2016;7:86.

# Figures

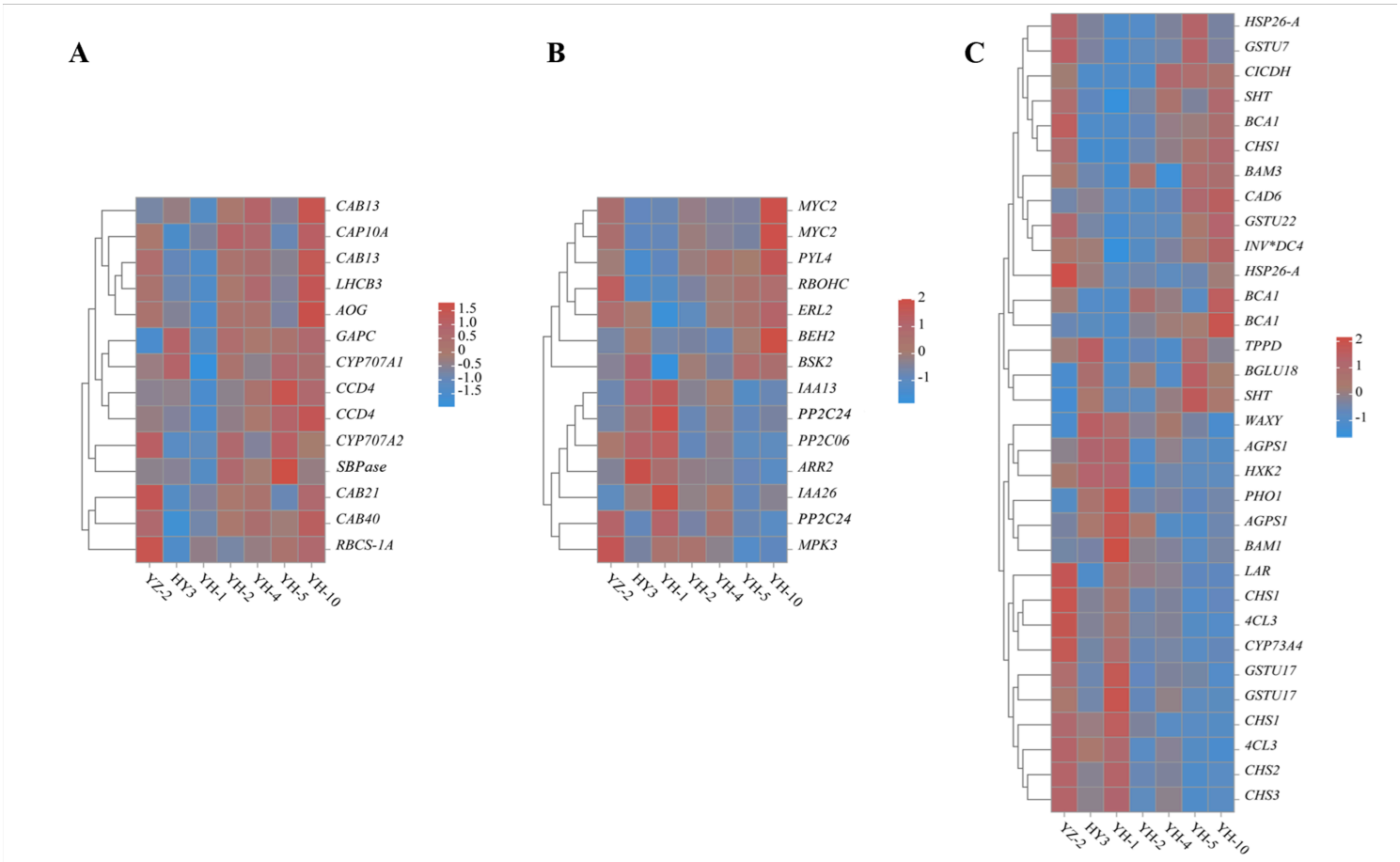


**Figure 3**

Heatmap of gene expression profiles associated with enriched KEGG signaling pathways. (A) Key DEGs related to the direct pathways of photosynthesis. (B) Key DEGs associated with hormone-related. (C) Other important DEGs associated with high photosynthetic efficiency.

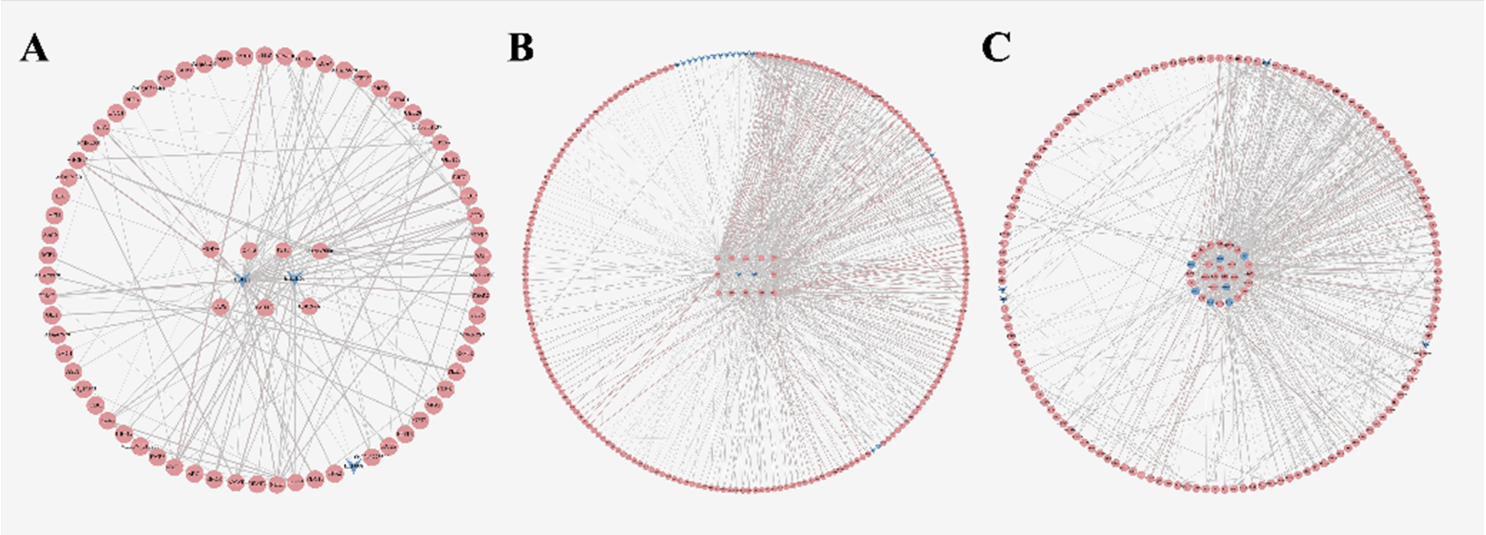
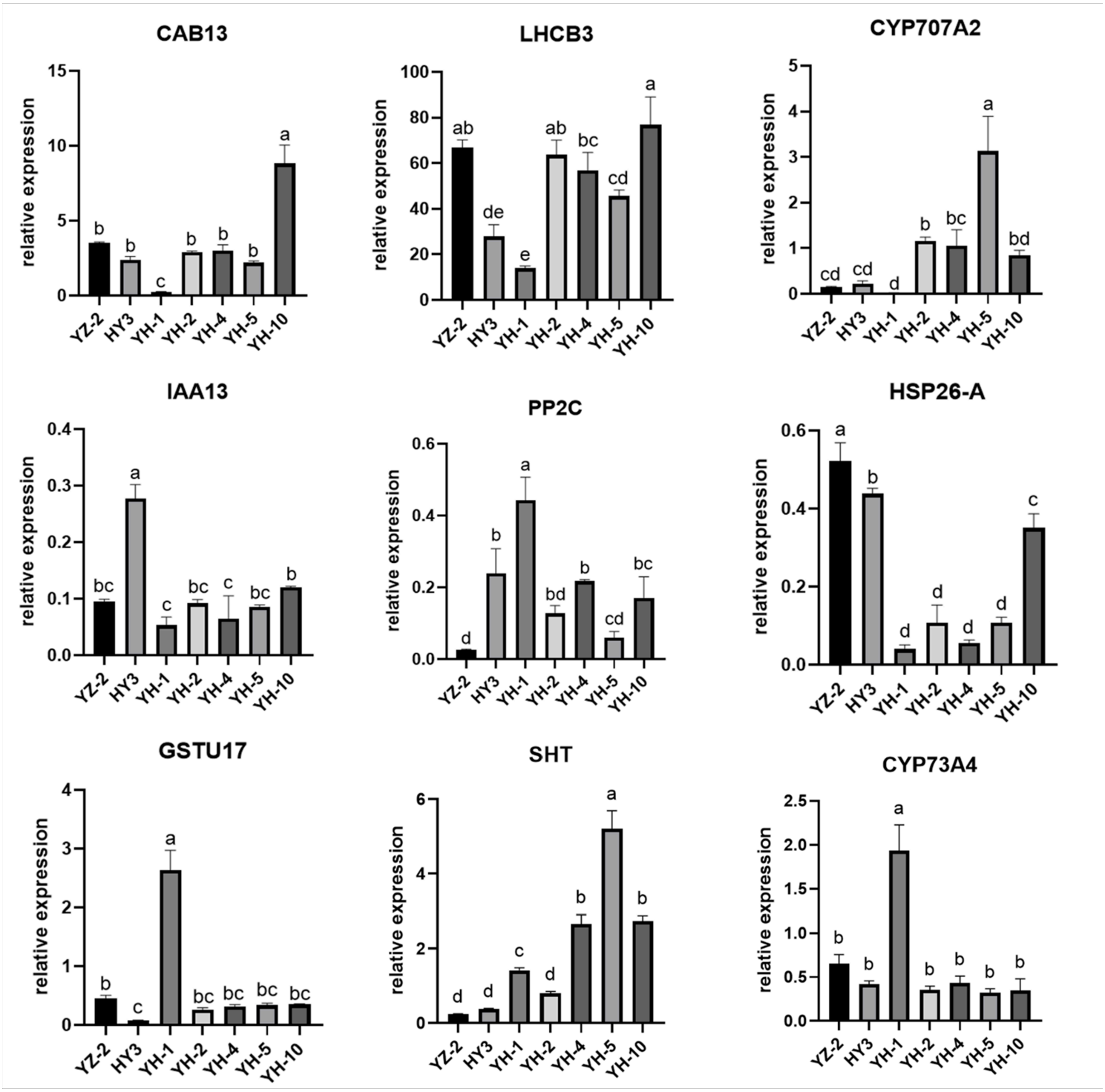



**Figure 5**

Co-expression networks of trait-associated modules. (A) darkseagreen3; (B) navajowhite1; (C) green.




## Figure 6

Quantitative real-time PCR (qRT-PCR) validation of candidate DEGs.

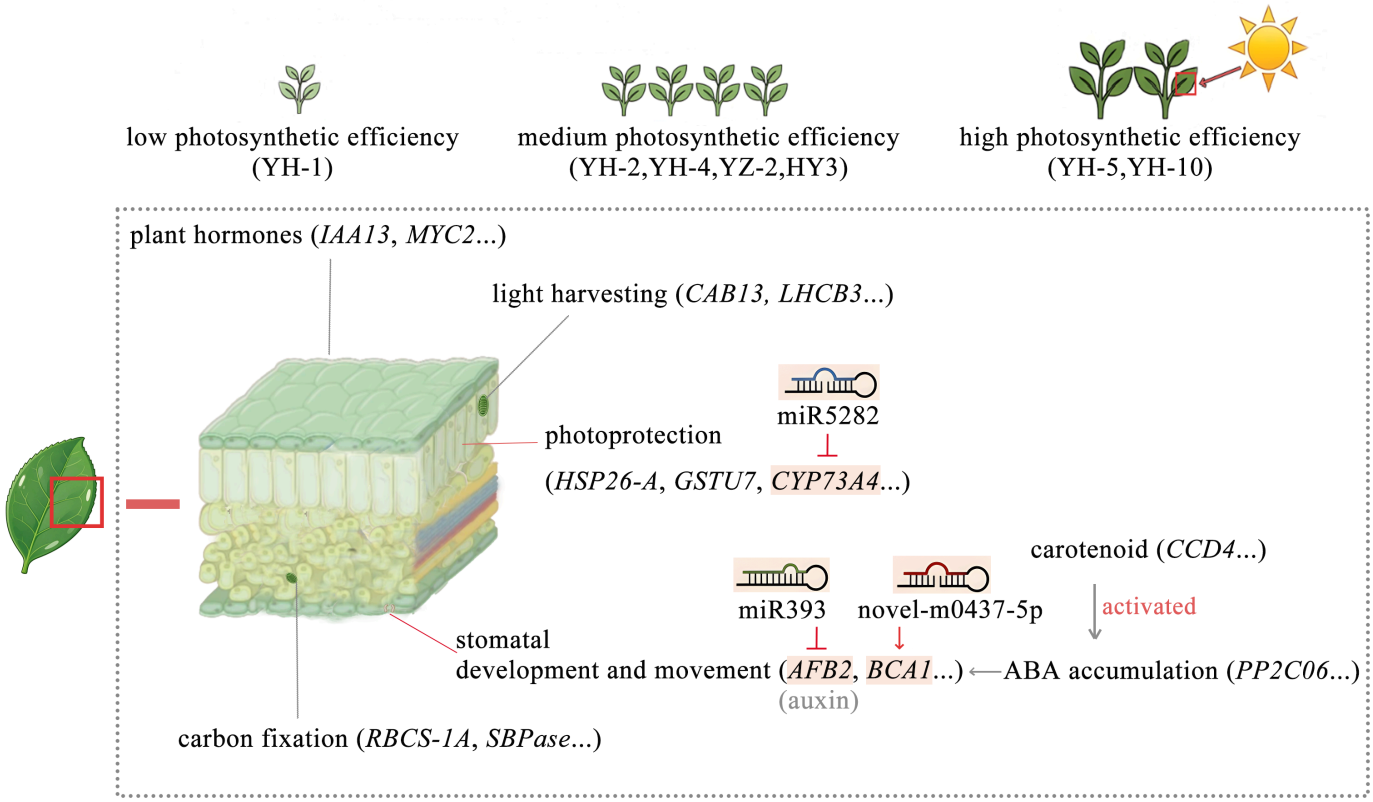



**Figure 8**

High photosynthetic efficiency molecular mechanism diagram.

## Supplementary Files

This is a list of supplementary files associated with this preprint. Click to download.

- Supplementarytables.docx
- Supplementaryfigures.docx